Applied Surface Science 464 (2019) 360–366

Contents lists available at ScienceDirect

Applied Surface Science

journal homepage: www.elsevier.com/locate/apsusc

Full Length Article

Tungsten self-organization nanowires prepared by DC magnetron sputtering

C.H. Verbeno[a], A.C. Krohling[a], T.C. Freitas[a], T.E.P. Bueno[a], M.A. Schettino Jr.[a], J.C. González[b], C. Larica[a], V.P. Nascimento[a], E.C. Passamani[a,*]

[a] Physics Department, Federal University of Espírito Santo, 29075-910 Vitória, Espírito Santo, Brazil
[b] Physics Department, Federal University of Minas Gerais, 30123-970 Belo Horizonte, Minas Gerais, Brazil

ARTICLE INFO

Keywords:
Sapphire corrugated surfaces
Surface morphology analysis
DC magnetron sputtering
Tungsten nanowires
Shadow effect

ABSTRACT

Tungsten nanowires were deposited by DC magnetron sputtering onto vicinal sapphire substrates with a specific geometry in which the entrance angle (solid angle) of the vapor beam relative to the substrate was modified. Through 2D auto-correlation function analysis, suitable conditions to obtain a nanoscale corrugated surface with a high-order correlation were determined concerning the annealing procedure (1300 °C for 5 h) of the sapphire substrates with miscut angle of 0.3°. Depending on the entrance angle of the tungsten vapor beam, different nanoparticles and/or nanowires were systematically produced under controlled conditions. AFM images, from the samples deposited with an entrance angle lower or equal to the miscut angle (0.3°) on the annealed sapphire substrates have shown homogeneous, uniform and isolated tungsten nanowires.

1. Introduction

Materials that have, at least, one relevant length scale within the range of nanometers [thin films (2D), nanowires (1D) or nanodots/nanoparticles (0D)] are commonly referred to as nanostructures. Due to discontinuities of the atomic translational symmetry found at the surfaces/interfaces, effects such as the reduction of atomic coordination and changes in the length and angle of chemical bonds, among others, are enhanced in these nanostructures, resulting in chemical and physical properties not found in their bulk states [1,2]. In particular, the use of nanowires (NWs) has been proposed in different technological applications in distinct areas, such as: optics [3–5], electronics [2,6,7], magnetism [8–11], and others. However, the production of NWs still presents a great challenge. Although known to have several shapes and sizes [3–11], NWs may be identified by two geometries: (i) free-standing NWs (grown out of the substrate plane), commonly prepared by the vapor-liquid-solid (VLS) mechanism [12], electrodeposition of metal on nanoporous matrices [13] or chemical routes [14], and (ii) the planar NWs (grown parallel to the substrate plane), usually produced by lithography [15], chemical routes [16] or grazing incidence deposition on nanostructured surfaces with 1D-ordering [17].

Molecular Beam Epitaxy (MBE) and Ion Beam Sputtering (IBS) are the two most used experimental methods for preparing planar NWs by grazing incidence vapor beam in a specific deposition geometry [8,17]. These authors employed the shadowing effect of the nanoripple patterns or vicinal surfaces to favor the deposition of materials at preferential regions of the substrate surface with the objective of producing NWs. Therefore, the growth of NWs follows a periodicity due to the lateral replication of the substrate's surface pattern. This procedure presents a great advantage when compared, for example, to the randomly oriented NWs prepared by chemical routes. Other advantages of this process are: (i) any type of substrates (oxides, metallic or semiconductors) can be used to prepare NWs and (ii) it's a single step process, while the NW fabrication using lithography requires multiple steps in addition to being a more expensive process.

Among different NWs materials, metallic tungsten nanowires (W-NWs) have recently attracted considerable attention due to their excellent field-emission properties [18,19]. Furthermore, tungsten oxide nanowires (WO_x-NWs) have demonstrated efficiency when used in photochemical devices [3], electrochromic or photochromic devices [6] and photo-electrolysis [14]. Considering (i) the potential application of tungsten (W) and (ii) that the magnetron sputtering method has not yet been applied, within our knowledge, for production of NWs due to its high deposition rate and non-collimated vapor beam as compared with the MBE setup, an experimental procedure using a sputtering setup is being proposed here to prepare W-NWs (or naturally WO_x-NWs) on corrugated substrates. Atomic Force Microscopy (AFM) was applied to study the vicinal surface formation of the sapphire substrates with miscut of 0.3° as well as the NWs formation on the step-edge of these vicinal surfaces. We have specifically investigated the influence of the vicinal surface's steps/terraces on the NWs arrangements.

* Corresponding author.
E-mail address: edson@cce.ufes.br (E.C. Passamani).

https://doi.org/10.1016/j.apsusc.2018.09.092
Received 21 June 2018; Received in revised form 6 September 2018; Accepted 10 September 2018
Available online 11 September 2018
0169-4332/

2. Experimental procedures

A sapphire wafer with a diameter of 51 mm, cut perpendicular to the [0 0 0 1] direction and with a miscut angle α = 0.3° towards the [1$\bar{2}$10] direction, was divided into several small pieces of 3 × 4 mm^2. These parts were cleaned following a sequence of baths: acetone, alcohol (isopropyl), and finally, deionized water. Subsequently, the cleaned and dried pieces were inserted in an air atmosphere furnace kept at temperatures T = 1000, 1100, 1200 and 1300 °C, during a timeτ = 5, 10, 15 and 20 h. As reported in literature [20], vicinal surfaces of sapphire substrates (terrace-width and step-height) are dependent on the miscut angle of the substrate, the annealing temperature and time. Thus, the aforementioned procedure was performed to investigate the kinetics involved in the vicinal structure formation of the sapphire substrate with α = 0.3° and, consequently obtain the suitable annealing temperature and time to form a regular and homogenous terrace-width/step-height distribution on the substrate surface. Atomic Force Microscopy (AFM) technique, using a Shimadzu SPM 9600 microscope operating at room temperature in contact mode, was applied immediately afterwards to study the annealed sapphire surfaces in order to reduce contaminants that could be adsorbed due to the long aging period. The thermal annealing procedure followed by the AFM analysis was repeated several times to ensure the reproducibility of the treatment. After that, the best annealing conditions to prepare W-NWs by DC magnetron sputtering were selected. A wedge was mounted on the sample-holder that was kept fixed (without rotation) during the deposition, as schematically shown in Fig. 1. The use of the wedge, with a suitable angle, enables a grazing incidence sputtered beam from the W target to reach the annealed sapphire substrate surfaces. Considering the vapor beam of W has a cone-like shape (Φ-solid angle of approximately 32°) and the vertical position of the sample can be set (sample holder relative to incident vapor beam), the entrance angle β of the deposition beam that reaches the substrate was geometrically estimated with a precision of ± 0.4°. In fact, the β value equal to zero was determined when no material reaches the substrate (seen by AFM), while different β values were obtained by vertical movement of the sample relative to Φ-solid angle, adjusted by a screw with precision under the 0.1 mm range. Firstly, we placed the substrate at the edge of the Φ-solid angle of the W vapor beam and one sample was deposited. Afterwards, we moved down the sample-holder to three predetermined vertical positions in order to vary β. Once again, a sample was prepared for each value of β.

When the beam is directed to the step edge of the substrate, the surface morphology of the deposited material will depend on the β- and α- angles. For β > α, as shown in Fig. 2a, the vapor deposition occurs on the terraces and a cluster-like structure may appear at the step-edge due to the *shadowing* effect. However, when β ≤ α, as displayed in Fig. 2b, the *shadowing* effect was enhanced, favoring the growth of planar NWs structures on the sapphire vicinal surface.

In particular, W-NWs were grown by grazing incident deposition for different values of β-angle at room temperature and under argon

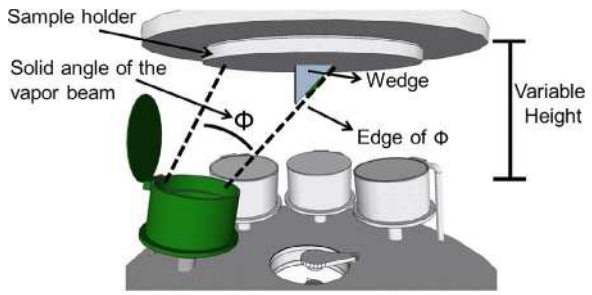

Fig. 1. Schematic picture of the AJA Orion 8 confocal magnetron sputtering used to deposit the tungsten sputtered beam under grazing incidence angle at the top of the step-and-terrace surface of the annealed sapphire.

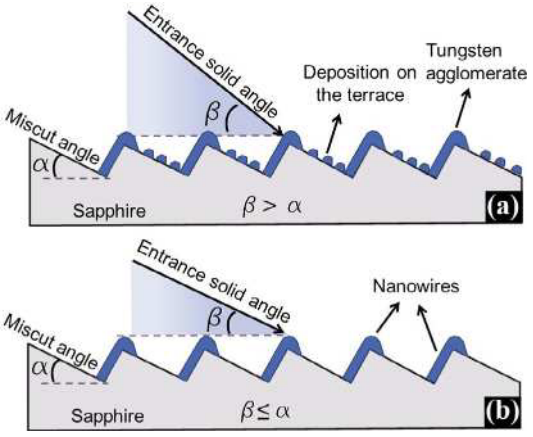

Fig. 2. Scheme for grazing incidence deposition onto vicinal surfaces. α is the miscut angle of the substrate, while β corresponds to the entrance angle between the edge of the sputtered beam and the sample surface: (a) β > α and (b) β ≤ α.

working pressure of 1.6 mTorr. Before the deposition, the base pressure in the chamber was 3 × 10^{-8} Torr. For β = 90°, a constant adatom flux φ of 0.011 nm/s was experimentally determined from the X-ray reflectivity curves of a 25 nm W film. It should be noted that X-ray diffraction patterns, recorded 3 months after the preparation of the 25 nm W film, still display Bragg peaks of metallic W. This observation indicates that the tungsten oxide layer, naturally formed during the ex-situ experiments, prevents full oxidation of the W film. Consequently, this result may also be expected in the NWs here discussed (no X-ray experiment was performed in our 3 × 4 mm^2 samples). Considering that the substrate was mounted in tilted configuration relative to the sputtered beam, the effective deposition rate (φ_{ef}) of W on the substrate is given by Eq. (1)

$$\varphi_{ef} = \varphi \cdot \sin\beta \quad (1)$$

Thus, the film thickness (σ) can be estimated as: $\sigma = \varphi_{ef} \cdot t$, where the t-parameter is the deposition time. Surface morphology and roughness of the deposited materials were studied by AFM. 2D-Auto-Correlation-Function (2D-ACF) analysis of the recorded AFM images was also performed.

3. Results and discussions

3.1. Sapphire substrate preparation: optimum annealing conditions

In order to study the kinetics of the vicinal surfaces on sapphire substrates with miscut angle α = 0.3°, heat treatments, for different T and τ values, were performed and the AFM results are shown in Fig. 3(a–q). 2D-Auto-Correlation Functions were obtained from the AFM images and are plotted as insets in Fig. 3. From the AFM images (or 2D-ACF), distinct vicinal surfaces (step-and-terrace-like morphologies) were obtained when T and τ-parameters were varied. As indicated in Fig. 3e, the facets' step-edges are parallel to the [10$\bar{1}$0] direction and perpendicular to the nominal miscut [1$\bar{2}$10] direction. An average angle of these facets was quantitatively measured to be close to 0.3°; a value about that of the sapphire substrate nominal miscut α-angle. It has also been confirmed that the main morphological characteristics are reproducible in all sample areas, indicating the annealed samples are homogeneous.

Overall, two types of vicinal structures can be observed in the AFM images. The first one (Fig. 3b) is formed by a set of single steps with heights *h* of 0.216 nm, and that corresponds to a 1/6 of the c-value of the sapphire unity cell (*c* = 1.299 nm) at the [0 0 0 1] direction [21]. The second vicinal structure, represented in Fig. 3n, displays step bunch formations or simply macro-steps. The step-bunching process can be

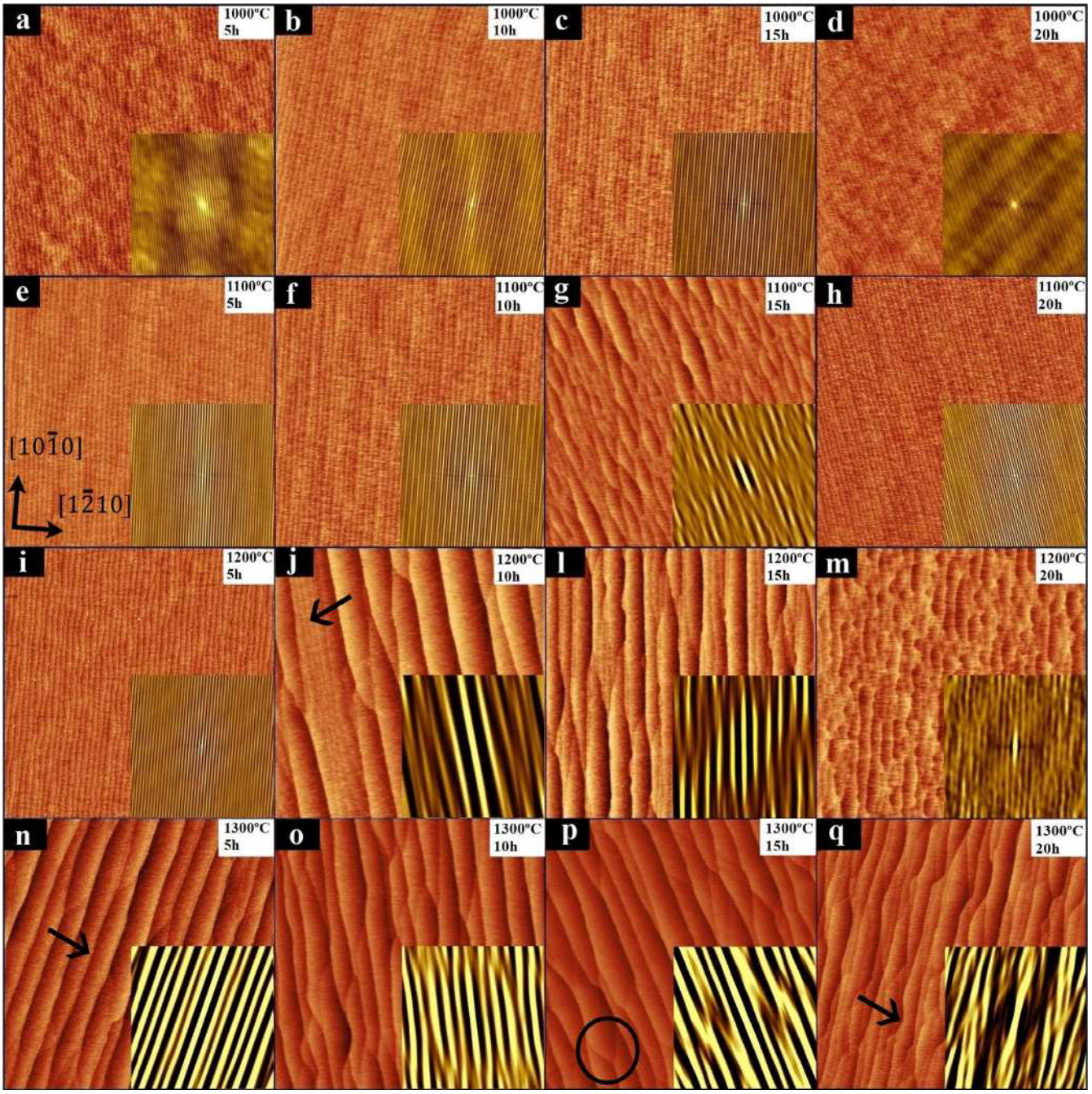

Fig. 3. AFM image (4 × 4 um^2) of the annealed sapphire substrates for 5, 10, 15 and 20 h at the temperatures of 1000 °C (a)–(d), 1100 °C (e)–(h), 1200 °C (i)–(m) and 1300 °C (n)–(q). The calculated 2D-ACF of the AFM images is inserted.

described as local changes of the step densities where two or more single steps of adjacent vicinal surfaces coalesce during the substrate annealing, leading to the formation of single macro-steps with heights multiple of $c/6$ [20,22,23]. Reported experimental results [20,24] suggest that step-bunching is a thermally activated process. In addition, our results indicate that the activation temperature of step-bunching may depend on the τ-parameter, since the τ-values (where the macro-steps are observed) reduce as the annealing temperature T increases [1100 °C/15 h (Fig. 3g); 1200 °C/10 h (Fig. 3j); 1300 °C/5h (Fig. 3n)].

Thus, on the one hand, for samples annealed at T ≤ 1200 °C, a morphological surface with un-concluded kinetics of the step-bunching process can be observed in the AFM images. As a result, the surface reveals an alternate sequence of macro-steps followed by a group of single steps (see the arrow in Fig. 3j). On the other hand, when annealed at 1300 °C, the step-bunching leads the sapphire surface to a morphology composed by macro-steps on the entire sample. These results can be explained assuming what is reported in the literature [24], where authors consider that step-bunching is an intermediate phenomenon that precedes the step-faceting process, and its disappearing rate is intrinsically related to the miscut angle of the sapphire substrate and T-values. Step-faceting is defined as a modification of a step fraction leading to its parallel value with a low crystallographic index direction [22,25]. As can be observed along the longitudinal direction of the macro-steps, the terraces are often blocked by coalescence junctions, as shown by the circles in Fig. 3p. In other words, surface areas where several steps are converging, favor steps with higher heights. From regions close to these “fusions”, the parallel steps change their directions, causing the faceting phenomenon; a process that

schematically follows a zipper-like movement [21,26]. Thus, the time-evolution of the sapphire morphology is conducted by total surface free energy minimization that is associated with the formation of new facets with different orientations and/or with fluctuation of the step-edges, as indicated by the arrow in Fig. 3q [27]. For longer annealing times, terraces with smaller lengths were observed. It seems that this observation is a characteristic of the annealed sapphire substrate prepared with miscut angle α smaller than < 0.6°, according to results reported in the literature [22,28].

Quantitative information on the order-degree and topographic surface anisotropies can be obtained by the analysis of the 2D-ACF in AFM images. As reported in the literature [29], any surface undulations with approximately uniform spacing will give rise to oscillations in 2D-ACF. Thus, the period of oscillations observed in the 2D-ACF profile, taken along the [1$\bar{2}$10] direction, corresponds to the lateral periodicity (*L*) of the step arrays. The lateral dispersion can be defined as Z = (σ/$\overline{L}$).100, where $\overline{L}$ is the average lateral periodicity and σ is the standard deviation, so that Z shows the extent of variability of the lateral periodicity in relation to an average value. In addition, the first maximum in the 2D-ACF profile, taken along the [10$\bar{1}$0] direction, allows extraction of the characteristic lateral correlation length (ε-parameter is obtained by fitting the decay of the first maximum of the 2D-ACF profile). Therefore, the ε-parameter is a quantitative length parameter to distinguish between short and long-range ordering in the surface morphology. Thus, it defines an average lateral distance along the [10$\bar{1}$0] direction from an arbitrary point in the sample, until the correlation in the arrangement of the structural units is lost [30]. Therefore, a large ε and low lateral dispersion indicate a vicinal structure with large-order-correlated periodic faceting. Fig. 4(a–c) displays the main parameters obtained from the analyses of the 2D-ACF recorded by the AFM (10 x 10 um^2): lateral correlation length (ε), lateral periodicity (*L*), and lateral dispersion (*Z*) as a function of time. In general, samples annealed for T ≤ 1100 °C present low values for the epsilon and *L*-parameters; as expected if one considers that the vicinal structures are mainly formed by single steps. On the other hand, for T = 1200 °C, larger values for the epsilon and *L*-parameters were calculated. For samples annealed at 1300 °C (Fig. 3n–q), the ε-parameter reduces as the time increases. With step-faceting activation on these surfaces, ε-parameter can be associated with coalescence junctions, once the macro-step order is lost in these places along the [10$\bar{1}$0] direction. Then, this behavior can be understood as an intensification of the step-faceting process that favors the increase of the junction densities as well as an increase of the fluctuations at step-edges that are related to the high values of the lateral dispersions *Z*, as displayed in Fig. 4c. As mentioned above, samples annealed at 1200 °C have shown large values for ε and *L* at τ = 10 h and 15 h; a fact that can be attributed to the step-bunching process. Therefore, it can be associated with the lateral periodicity *L* of the terraces once they promote the formation of macro-steps with larger widths. However, for these conditions (1200 °C and 10 and 15 h) of annealing, a lateral dispersion is relatively high (about 40%), because the step-bunching process is not complete over the entire sample surface. Finally, for an annealing at 1300 °C lasting 5 h (Fig. 3n), the 2D-ACF parameters indicate vicinal structures with macro-steps strongly correlated with low lateral dispersion. Such result confirms the long-range 1D uniformity of the periodic surface corrugation and, consequently, the suitable annealing condition for sapphire substrate with a miscut of 0.3°. The annealing procedure was repeated five times to confirm the reproducibility of the kinetics responsible for the step-and-terrace formation.

3.2. Self-organization of nanowires on step-and-terrace sapphire substrate

As mentioned above, AFM image of the sapphire annealed at 1300 °C for 5 h (Fig. 5a) presents an organized and well distributed step-and-terrace feature, with the steps' height within the range of 0.4–0.9 nm, a lateral periodicity (*L)* of 323 nm and an average surface root-mean square roughness (R_{rms}) of about 0.1 nm. Different morphologies (obtained by AFM) of the W deposited for 1 h on the annealed sapphire, are shown in Fig. 5(b–e). The depositions were done by varying the amount of W atoms that reach the substrate by setting the entrance β-solid angle [according to Eq. (1)] in values of 57°; 5°; 2°; 0.3°, as indicated in Fig. 5. Line profiles of the AFM images (regions indicated in images) are plotted at the right-hand side of Fig. 5. It is important to note that the lateral broadening of the NW profiles, due to the tip-sample convolution [31], was evaluated. By means of considerations reported in Ref. [32], the convolution error was estimated to be ~3 nm. This result is consistent since the height of NWs is small and the working tip has steep edges (nominal angle of ~82°), consequently the foremost apex of the AFM tip is involved in imaging [31]. Therefore, the widths of NWs that will be presented in this work were corrected by this value. For the deposition with β = 57° (Fig. 5b), it can be noticed that the deposited W "layer" shows a surface with a vicinal structure *L* of 320 nm and a roughness similar to that of the substrate, i.e., the R_{rms} value of 0.1 nm, and steps at the interval of 0.4 to 0.9 nm. These results may indicate a non-equilibrium growth mechanism due to a high deposition rate and relatively low substrate temperature [33]. When β = 5° (Fig. 5c), the surface morphology starts to present the formation of quasi-spherical W nanoparticles (NPs) on the terraces and with a roughness of 0.7 nm, indicating that the growth mechanism leads to the formation of islands on the terraces (the surface energy of the sapphire\vacuum interface is smaller than the sapphire\W interface). In other words, according to Eq. (1), when the β-solid angle value reduces, there is a decrease of the deposition rate, favoring the atomic relaxation process to positions corresponding to the minimum potential energy; a mechanism that is characteristic of this deposition growth [33]. For β = 2° (Fig. 5d), it can be observed that the surface formed by W NPs on the terraces has a R_{rms} value of 0.5 nm. In addition, there is a formation of atomic clusters due to the *shadowing* effect [34], clearly seen in the respective height profile. Considering that the W sputtered beam is oriented, there is a geometric interaction among the incident

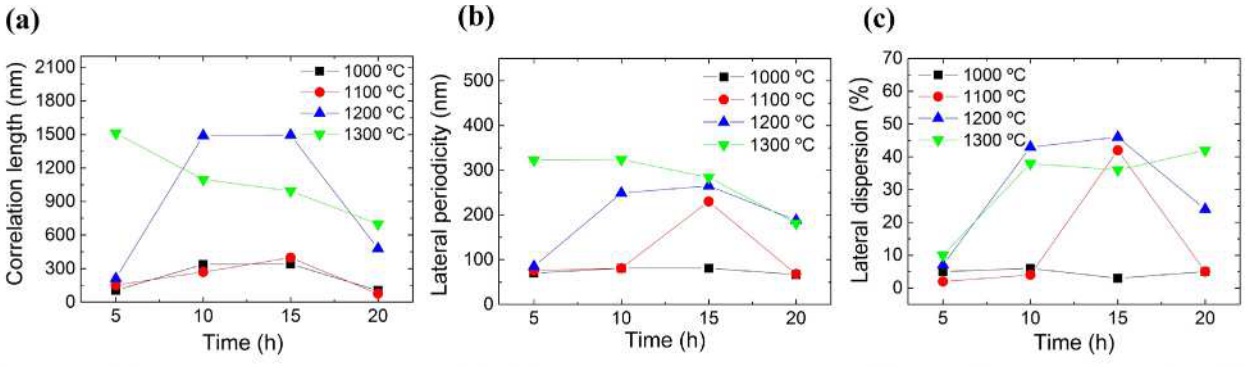

Fig. 4. (a) Lateral correlation length (ε), (b) average lateral periodicity (*L*) and (c) lateral dispersion (*Z*) obtained through ACF analysis in AFM images (10 × 10 μm^2).

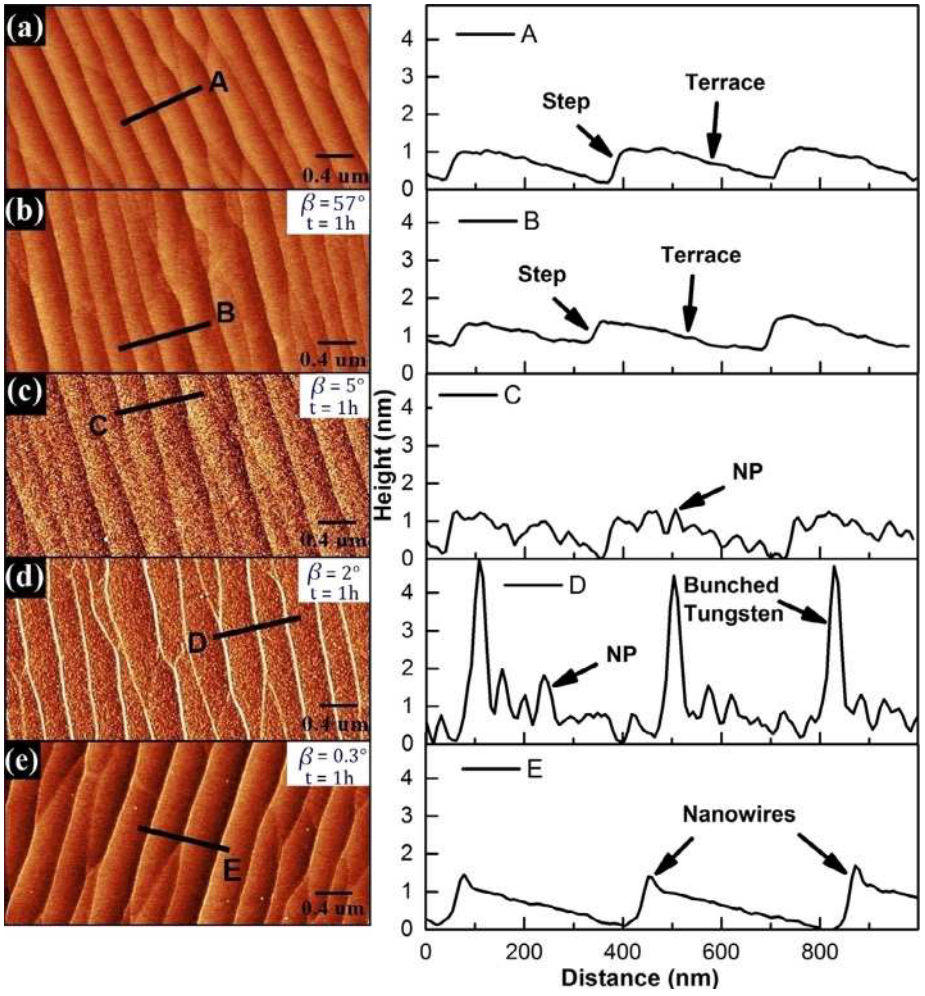

Fig. 5. Left-hand side: AFM images ($4 \times 2\,\mu m^2$) (a) of the sapphire substrate annealed at 1300 °C for 1 h and with tungsten deposited during 1 h but with different β solid angles (β = 57°; 5°; 2°; 0.3°, respectively) (b–e). Right-hand side: transversal line profile of heights as detached in the AFM images of the left-hand side.

adatoms and the *step-edges* of the sapphire surface that favors the formation of W-clusters; in this case, with a height of 4.5 nm and average width of 35 nm along the step-edges. Finally, when the angle is β = 0.3° (condition of β ≤ α), the deposited W goes mainly to the step edges, resulting in a planar nanostructured material (nanowires) along the sapphire vicinal surface (Fig. 5e). From Fig. 5 (right-hand side), the W-NWs have their heights at 1.3 nm and a width of 27 nm.

In order to understand the effect of deposition time on W nanowire formation, we prepared additional samples where the W deposition was done for β = 0.3°, during 0.5 h (a) and 2 h (b). The results are displayed in Fig. 6. From this figure, it is clear that the change in the deposition time modifies the W-NWs sizes, as shown in Figs. 5e and 6(a-b). More precisely, when the W is deposited during 0.5 h and 2.0 h, the average height and width of the formed NWs are, respectively: 1.2 nm and 24 nm or 2.2 nm and 36 nm. These values are different from those obtained with deposition of 1 h, as previously described. Thus, we can control the NWs sizes by performing deposition with DC sputtering under the condition of β ≤ α and changing the deposition time. It is worth noticing that the relationship between the effective deposited thickness (σ_{eff}) and the NW's volume is not linear. This fact can be attributed to the self-shadowing effect of NW, since the increase in height of the NWs leads to an intensification of the barriers where the incident W atoms is deposited. Finally, Fig. 6e presents a comparison of the height profile of the W-NWs with the sapphire substrate, where a preferential deposition of W on specific regions of the substrate vicinal surface can be observed. This phenomenon can be attributed to some factors: (i) the enhancement of the shadowing effect, because the step shadowing produces areas where the incident W atoms cannot reach; (ii) the mobility of the adatoms is relatively low at room temperature, inhibiting surface atomic diffusion that could occupy possible surface/interface vacancies; (iii) the low deposition rate for β = 0.3° favors the atomic relaxation process to positions corresponding to the minimum potential energy, then the atomic step edges, possessing several regions of high bonding degree, induce the nucleation. Hence, W atoms will preferentially be deposited on the step-edges of the sapphire surface, as displayed in Fig. 7.

4. Conclusion

We have studied the surface morphology of the (0 0 0 1) sapphire substrates [with miscut of 0.3°] submitted to annealing over a broad temperature range (from 1000 to 1300 °C) and different annealing time (5, 10, 15 and 20 h). Considering the 2D-Auto-Correlation Function of the AFM data, it has been established that annealing the sapphire at 1300 °C during 5 h results in a suitable vicinal surface structure; where the data show reproducible well-distributed and homogenous step-and-terraces (the procedure was repeated 5 times and the results were similar). Thus, a suitable annealed substrate to prepare controlled and auto-organized W-NWs using DC magnetron sputtering with a relatively high deposition rate was used. Based on the shadowing effect [35], an experimental procedure to deposit nanowires in magnetron sputtering setups that operate in confocal geometry has been developed (one is

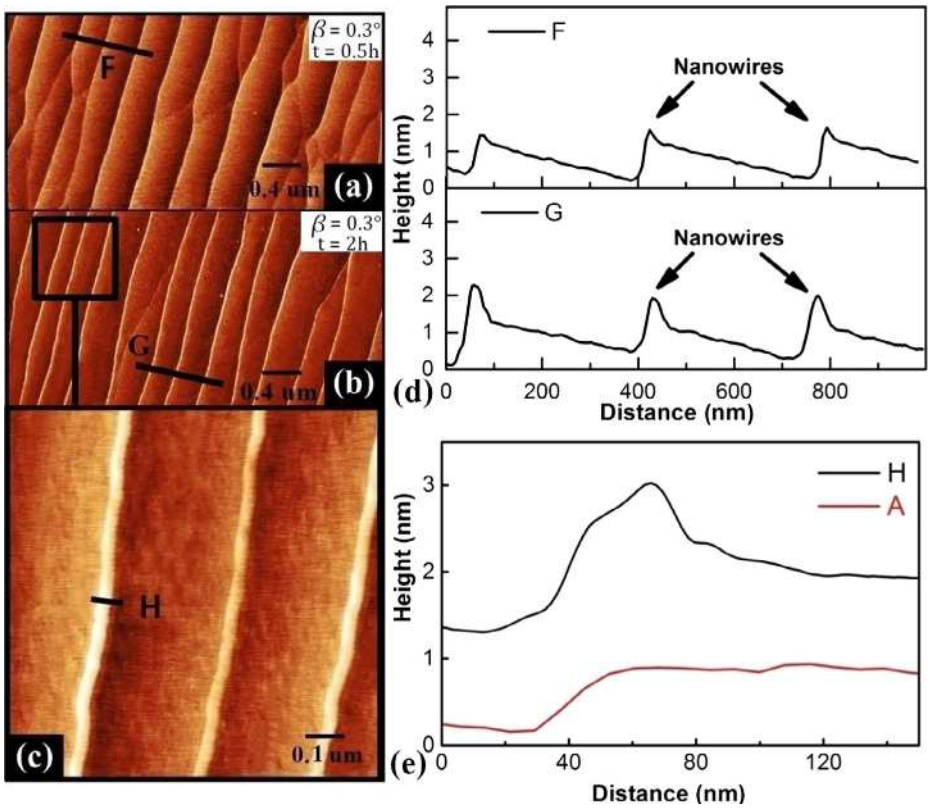

Fig. 6. AFM images ($4 \times 2\,\mu m^2$) of tungsten grown for β = 0.3° (around the miscut value of our sapphire substrate) at different deposition times: (a) 0.5 h and (b) 2 h. In (c) the AFM image ($1 \times 1\,\mu m^2$) of the area delimitated in (b) is shown. In (d) one shows the line profile of the AFM image. In (e) one compares the profiles of sapphire substrate (A) and the W-NWs (H).

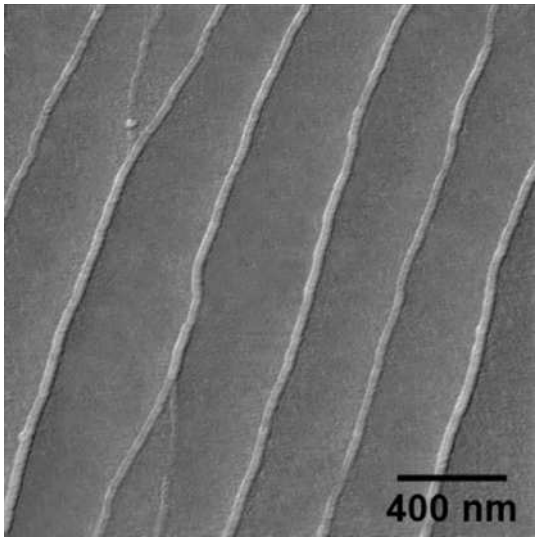

Fig. 7. AFM deflection signal image ($2 \times 2\,\mu m^2$) of tungsten grown for β = 0.3° during 2 h on sapphire substrate annealed at 1300 °C.

able to change the deposition rate that reaches the substrate, just by varying the entrance angle β of the deposition beam). Through this procedure, either W-NWs of different sizes (height and widht) or W-NPs (or a mixtures of NPs and NWs) were prepared. The NWs with different sizes were obtained when, in experimental conditions, the β-value was close to, or smaller than, the miscut α-angle of the sapphire substrate while concomitantly changing the deposition time. During the NWs depositons, the substrate atomic steps shadow subadjacent terraces, limiting the W sputtered beam that will preferencially be deposited alongside the step edges. Therefore, we have demonstrated that an incident vapor beam of the DC magnetron sputtering can restrict the deposition to a certain substrate region by basically changing the substrate position relative to the β-angle. Overall, our results are similar to those found when the nanowires were produced by IBS and MBE setups [17,8]. On the one hand, in an MBE setup a highly collimated molecular beam can be achieved by using a large working distance between the substrate and the evaporation source [17]. The molecular beam is then directed to the ascending step direction of vicinal surfaces, consequently the atoms form a NW structure on an open area along the step edges, at a deposition rate of the 10^{-3} nm/s order [17]. On the other hand, in an IBS setup [8] periodic NW structures can be deposited at a rate of about 10^{-2} nm/s by glancing-angle codeposition of Fe and Pt with a fixed angle of 5° on alumina nanoripple patterns [8]. However, in our work, a magnetron sputtering setup, operating in a specific deposition configuration (placing the substrate at the edge of the vapor beam cone), allowed to limit the amount of atomic vapor that reaches the vicinal surface, enabling the deposition of NWs with a relative low rate, similar to MBE configuration with an oriented beam [17]. In the present work, NWs were prepared with W deposited in a condition of β = 0.3°, with the following dimensions: heights of 1.2; 2.3 and 2.2 nm and average widths of 24; 27 and 36 nm, from deposition times of 0.5; 1 and 2 h, respectively.

Acknowledgments

The authors of this paper are immensely grateful for the financial support provided by the following Brazilian agencies: FAPES, CNPq and CAPES. We also thank the CNPEM for providing us with the infrastructure to cut the sapphire wafers at LNNano/LMF laboratory (Projects N° LMF-18746 and N° LMF-23162).

References

[1] B. Cullity, C. Graham, Introduction to Magnetic Materials, second ed., Wiley-IEEE Press, New Jersey, USA, 2009.

[2] Z.L. Wang, Nanowires and Nanobelts: Materials, Properties and Devices. Volume 1: Metal and Semiconductor Nanowires, Springer Science & Business Media, New York, USA, 2013. https://doi.org/10.1007/978-0-387-28747-8.

[3] G. Xi, S. Ouyang, P. Li, J. Ye, Q. Ma, N. Su, H. Bai, C. Wang, Ultrathin W18O49 Nanowires with diameters below 1 nm: synthesis, near-infrared absorption, photoluminescence, and photochemical reduction of carbon dioxide, Angew. Chem. Int. Ed. 51 (2012) 2395–2399, https://doi.org/10.1002/anie.201107681.
[4] O. Ualibek, R. Verre, B. Bulfin, V. Usov, K. Fleischer, J.F. McGilp, I.V. Shvets, Manipulating and probing the growth of plasmonic nanoparticle arrays using light, Nanoscale. 5 (2013) 4923–4930, https://doi.org/10.1039/c3nr00087g.
[5] L. Cao, P. Fan, A.P. Vasudev, J.S. White, Z. Yu, W. Cai, J.A. Schuller, S. Fan, M.L. Brongersma, Semiconductor nanowire optical antenna solar absorbers, Nano Lett. 10 (2010) 439–445, https://doi.org/10.1021/nl9036627.
[6] J. Wang, E. Khoo, P.S. Lee, J. Ma, Synthesis, assembly, and electrochromic properties of uniform crystalline WO_3 nanorods, J. Phys. Chem. C. 112 (2008) 14306–14312, https://doi.org/10.1021/jp804035r.
[7] J. Liu, Z. Zhang, Y. Zhao, X. Su, S. Liu, E. Wang, Tuning the field-emission properties of tungsten oxide nanorods, Small. 1 (2005) 310–313, https://doi.org/10.1002/smll.200400054.
[8] M. Garel, D. Babonneau, A. Boulle, F. Pailloux, A. Coati, Y. Garreau, A. Ramos, C. Tolentino, Self-organized ultrathin FePt nanowires produced by glancing-angle ion-beam codeposition on rippled alumina surfaces, Nanoscale 7 (2015) 1437–1445, https://doi.org/10.1039/C4NR05589F.
[9] A.V. Ognev, K.S. Ermakov, A.Y. Samardak, A.G. Kozlov, E.V. Sukovatitsina, A.V. Davydenko, L.A. Chebotkevich, A. Stancu, A.S. Samardak, Self-organization and FORC-based magnetic characterization of ultra-high aspect ratio epitaxial Co nanostrips produced by oblique deposition on an ordered step-bunched silicon surface, Nanotechnology 28 (2017) 095708, https://doi.org/10.1088/1361-6528/aa564e.
[10] S.K. Arora, B.J. Odowd, B. Ballesteros, P. Gambardella, I.V. Shvets, Magnetic properties of planar nanowire arrays of Co fabricated on oxidized step-bunched silicon templates, Nanotechnology 23 (2012) 235702, https://doi.org/10.1088/0957-4484/23/23/235702.
[11] I.V. Shvets, H.C. Wu, V. Usov, F. Cuccureddu, S.K. Arora, S. Murphy, Concept of a nanowire array magnetoresistance device, Appl. Phys. Lett. 92 (2008) 023107, https://doi.org/10.1063/1.2834371.
[12] N.J. Quitoriano, T.I. Kamins, Using pn junction depletion regions to position epitaxial nanowires, J. Appl. Phys. 102 (2007) 044311, https://doi.org/10.1063/1.2770820.
[13] L.F. Liu, S.S. Xie, W.Y. Zhou, From Co/Pt multilayered nanowires to Co-Pt alloy nanowires: Structural and magnetic evolutions with annealing temperatures, J. Phys. D. Appl. Phys. 42 (2009) 205002, https://doi.org/10.1088/0022-3727/42/20/205002.
[14] J. Su, X. Feng, J.D. Sloppy, L. Guo, C.A. Grimes, Vertically aligned WO_3 nanowire arrays grown directly on transparent conducting oxide coated glass: synthesis and photoelectrochemical properties, Nano Lett. 11 (2011) 203–208, https://doi.org/10.1021/nl1034573.
[15] S. Goolaup, A.O. Adeyeye, N. Singh, G. Gubbiotti, Magnetization switching in alternating width nanowire arrays, Phys. Rev. B – Condens. Matter Mater. Phys. 75 (2007) 144430, https://doi.org/10.1103/PhysRevB.75.144430.
[16] Z. Gu, Y. Ma, W. Yang, G. Zhang, J. Yao, Self-assembly of highly oriented one-dimensional h-WO_3 nanostructures, Chem. Commun. (2005) 3597–3599, https://doi.org/10.1039/b505429j.
[17] F. Cuccureddu, V. Usov, S. Murphy, C.O. Coileain, I.V. Shvets, Planar nanowire arrays formed by atomic-terrace low-angle shadowing, Rev. Sci. Instrum. 79 (2008) 053907, https://doi.org/10.1063/1.2929835.
[18] C.L. Chen, K. Arakawa, H. Mori, Two-dimensional metallic tungsten nanowire network fabricated by electron-beam-induced deposition, Nanotechnology 21 (2010) 285304, https://doi.org/10.1088/0957-4484/21/28/285304.
[19] K.S. Yeong, J.T.L. Thong, Field-emission properties of ultrathin 5 nm tungsten nanowire, J. Appl. Phys. 100 (2006) 114325, https://doi.org/10.1063/1.2400722.
[20] F. Cuccureddu, S. Murphy, I.V. Shvets, M. Porcu, H.W. Zandbergen, N.S. Sidorov, S.I. Bozhko, Surface morphology of c-plane sapphire (α-alumina) produced by high temperature anneal, Surf. Sci. 604 (2010) 1294–1299, https://doi.org/10.1016/j.susc.2010.04.017.
[21] O. Kurnosikov, L. Pham Van, J. Cousty, About anisotropy of atomic-scale height step on (0001) sapphire surface, Surf. Sci. 459 (2000) 256–264, https://doi.org/10.1016/S0039-6028(00)00452-0.
[22] L. Pham Van, O. Kurnosikov, J. Cousty, Evolution of steps on vicinal (0001) surfaces of α-alumina, Surf. Sci. 411 (1998) 263–271, https://doi.org/10.1016/S0039-6028(98)00329-X.
[23] D. Zhang, Y. Gan, Effects of plasma treatment on evolution of surface step-terrace structure of critically cleaned c-plane sapphire substrates: An AFM study, Appl. Surf. Sci. 285 (2013) 211–214, https://doi.org/10.1016/j.apsusc.2013.08.038.
[24] O. Kurnosikov, L. Pham Van, J. Cousty, High-temperature transformation of vicinal (0001) Al_2O_3-α surfaces: An AFM study, Surf. Interface Anal. 29 (2000) 608–613, https://doi.org/10.1002/1096-9918(200009)29:9<608::AID-SIA906>3.0.CO;2-B.
[25] J.R. Heffelfinger, M.W. Bench, C.B. Carter, Steps and the structure of the (0001) α-alumina surface, Surf. Sci. 370 (1997) L168–L172, https://doi.org/10.1016/S0039-6028(96)01123-5.
[26] J.R. Heffelfinger, C.B. Carter, Mechanisms of surface faceting and coarsening, Surf. Sci. 389 (1997) 188–200, https://doi.org/10.1016/S0039-6028(97)00411-1.
[27] C. Misbah, O. Pierre-Louis, Y. Saito, Crystal surfaces in and out of equilibrium: A modern view, Rev. Mod. Phys. 82 (2010) 981–1040, https://doi.org/10.1103/RevModPhys. 82.981.
[28] P.R. Ribič, G. Bratina, Behavior of the (0 0 0 1) surface of sapphire upon high-temperature annealing, Surf. Sci. 601 (2007) 44–49, https://doi.org/10.1016/j.susc.2006.09.003.
[29] H. Assender, V. Bliznyuk, K. Porfyrakis, How surface topography relates to materials' properties, Science 297 (2002) 973–976, https://doi.org/10.1126/science.1074955.
[30] V. Bliznyuk, Vi. Burlakov, H. Assender, G.A.D. Briggs, Y. Tsukahara, Surface structure of amorphous PMMA from SPM: auto-correlation function and fractal analysis, Macromol. Symp. 167 (2001) 89–100, https://doi.org/10.1002/1521-3900(200103)167:1<89::AID-MASY89>3.0.CO;2-S.
[31] J. Shen, D. Zhang, F. Zhang, Y. Gan, AFM tip-sample convolution effects for cylinder protrusions, Appl. Surf. Sci. 422 (2017) 482–491, https://doi.org/10.1016/j.apsusc.2017.06.053.
[32] J. Canet-Ferrer, E. Coronado, A. Forment-Aliaga, E. Pinilla-Cienfuegos, Nanotechnology. 25 (2014) 395703, https://doi.org/10.1088/0957-4484/25/39/395703.
[33] A. Guimarães, Principles of Nanomagnetism, first ed., Springer, New York, USA, 2009. https://doi.org/10.1007/978-3-642-01482-6.
[34] D. Vick, L.J. Friedrich, S.K. Dew, M.J. Brett, K. Robbie, M. Seto, T. Smy, Self-shadowing and surface diffusion effects in obliquely deposited thin films, Thin Solid Films 339 (1999) 88–94, https://doi.org/10.1016/S0040-6090(98)01154-7.
[35] A.C. Krohling, T.E.P. Bueno, V.P. Nascimento, C. Larica, K. Krambrock, D. Menzel, F.J. Litterst, E.C. Passamani, Spin valve heterostructures built using the shadowing effect: Setting NiFe and Co magnetization directions for non-collinear couplings, Appl. Phys. Lett. 111 (2017) 262404, https://doi.org/10.1063/1.5003220.